Fast vision-based catheter 3D reconstruction

2016 Phys. Med. Biol. 61 5128

(http://iopscience.iop.org/0031-9155/61/14/5128)

IOP Publishing | Institute of Physics and Engineering in Medicine Physics in Medicine & Biology

Phys. Med. Biol. **61** (2016) 5128–5148 doi:10.1088/0031-9155/61/14/5128

Fast vision-based catheter 3D reconstruction

Mohsen Moradi Dalvand[1,2], **Saeid Nahavandi**[1] **and Robert D Howe**[2]

[1] Institute for Intelligent Systems Research and Innovation (IISRI), Deakin University, Victoria 3216, Australia

[2] Harvard Paulson School of Engineering and Applied Sciences, Cambridge, MA 02138, USA

E-mail: mdalvand@seas.harvard.edu

Received 20 October 2015, revised 28 April 2016
Accepted for publication 16 May 2016
Published 28 June 2016

Abstract

Continuum robots offer better maneuverability and inherent compliance and are well-suited for surgical applications as catheters, where gentle interaction with the environment is desired. However, sensing their shape and tip position is a challenge as traditional sensors can not be employed in the way they are in rigid robotic manipulators. In this paper, a high speed vision-based shape sensing algorithm for real-time 3D reconstruction of continuum robots based on the views of two arbitrary positioned cameras is presented. The algorithm is based on the closed-form analytical solution of the reconstruction of quadratic curves in 3D space from two arbitrary perspective projections. High-speed image processing algorithms are developed for the segmentation and feature extraction from the images. The proposed algorithms are experimentally validated for accuracy by measuring the tip position, length and bending and orientation angles for known circular and elliptical catheter shaped tubes. Sensitivity analysis is also carried out to evaluate the robustness of the algorithm. Experimental results demonstrate good accuracy (maximum errors of ± 0.6 mm and ± 0.5 deg), performance (200 Hz), and robustness (maximum absolute error of 1.74 mm, 3.64 deg for the added noises) of the proposed high speed algorithms.

Keywords: catheter, 3D reconstruction, vision-based reconstruction, continuum robots

(Some figures may appear in colour only in the online journal)

1. Introduction

Continuum robots are continuously curving manipulators that have distributed deformation along their length with theoretically an infinite number of degrees of freedom (DOF) (Trivedi *et al* 2008). They are inspired by biological continuum structures like elephant trunks, octopus arms, squid tentacles and snakes (Jones and Walker 2006, Andruska and Peterson 2008, Ning and Worgotter 2012). Compared to traditional rigid-link robots, continuum robots offer advantages including better maneuverability and inherent compliance (Trivedi *et al* 2008). This makes them well-suited for a variety of applications from industrial inspection to minimally invasive surgery (MIS) where instruments must navigate gently through tissues (Camarillo *et al* 2008a, Ding *et al* 2013, Polygerinos *et al* 2013, Burgner *et al* 2014). Our primary motivation for the vision-based 3D reconstruction algorithm described in this paper is continuum robots used in catheter and endoscopic procedures where the tip of the catheters or endoscopes must be controlled in real-time. This is especially challenging when motion compensation is used to repair fast moving intracardiac structures (Kesner and Howe 2011).

While there has been considerable progress in the area of actuation strategies for such robots (Gravagne *et al* 2003), the problem of 3D shape sensing is still a challenge (Camarillo *et al* 2009). A few indirect methods relating internal actuator parameters to the tip position have been proposed in the literature to estimate the shape of continuum robots (Hannan *et al* 2001, Jones and Walker 2006). These methods do not have accuracies (average error 17.4% to 57.4%) comparable to position sensing in rigid link robots (Chitrakaran *et al* 2004). Different techniques have been proposed for directly measuring the tip position and also sensing the 3D shape of these flexible robots by using strain sensors (Leleu *et al* 2001, Lee *et al* 2008) and fiber optic sensors (Grattan and Sun 2000, Cusano *et al* 2004). Fiber Bragg grating sensors have also been demonstrated, but this sensing technology can be expensive (Park *et al* 2010, Roesthuis *et al* 2014). Furthermore, due to the size limitations particularly for medical applications, applying these types of sensors can be difficult.

As a result, vision-based shape sensing approaches have gained attention for quantifying the articulation of continuum robots and catheters (Camarillo *et al* 2009). Vision-based approaches may also reduce costs, because they do not require transducers embedded in disposable catheters. One of the most popular and relatively straightforward vision-based methods is the use of body- and/or tip-mounted fiducial markers that are generally useful for non-medical applications (Chen *et al* 2003, Hannan and Walker 2003, 2005, Chitrakaran *et al* 2004, Webster *et al* 2009, Rucker 2011). Although fiducial markers simplify the reconstruction process by detecting the point correspondences in stereo vision systems, the fabrication of the markers that meet size, shape and visibility constraints is difficult. Moreover, the extraction of the central point of the marker bands using image processing techniques can be challenging.

Vision-based techniques were also employed for the shape sensing and position control of continuum robots in surgical field without using fiducial markers. Position control, manipulation and study of the steerable needles was one area that has gained considerable attention (Webster *et al* 2005, 2006, Glozman and Shoham 2007, Kallem and Cowan 2007, Alterovitz *et al* 2008, Kallem *et al* 2009, Ma *et al* 2012, Panayiotou *et al* 2013, 2015, Haase *et al* 2014). 3D reconstruction of a catheter shape by finding epipolar correspondence in two nearby x-ray views (2° apart) was proposed (Lee and Poston1997, Bender *et al* 1999). While accurate and robust, this method is not efficient and fast as it requires a brute force search of all points in one image for every point in the other using epipolar geometry to establish point correspondences (Lee and Poston1997).

A voxel-carving algorithm built upon the shape-from-silhouette technique was proposed to estimate and register the 3D shape of a catheter robot (Camarillo *et al* 2008a, 2008b, Camarillo *et al* 2009). The iterative reconstruction approach based on the extension of affine shape of finite point configurations from a number of uncalibrated cameras was also proposed (Berthilsson and Astrom 1997, Berthilsson *et al* 1997). Self-organizing map (SOM) and growing self-organizing maps (GSOM) structures (Kohonen 1990, Fritzke 1996, Kumar *et al* 2004, Croom *et al* 2010) as well as the improved version of SOM called 'stereo SOM' (Croom *et al* 2010) were investigated for finding the simplified curve approximating the 3D shape of continuum robots. Although these methods are generally straightforward to implement and relatively robust, they can be time-consuming (Camarillo *et al* 2008b), computationally expensive (Croom *et al* 2010), and complex (Berthilsson and Astrom 1997).

The approach of 3D reconstruction of a quadratic curve by using two or more corresponding conics produced by projecting the curve onto image planes under perspective transformation was also studied (Safaee-Rad *et al* 1992, Xie and Thonnat 1992, Kanatani and Liu 1993, Xie 1994, Kahl and Heyden 1998, Balasubramanian *et al* 2002, Yang *et al* 2014). It has been proved that analytical formulation with a unique solution from the roots of a quadratic equation can be obtained without point correspondences between the curves (Safaee-Rad *et al* 1992, Xie and Thonnat 1992, Balasubramanian *et al* 2002). This appealing approach seems to be computationally fast and well-suited for the 3D reconstruction of continuum robots and catheters in clinical conditions. Our focus in this study is to extend and implement this approach and investigate its capabilities in 3D shape sensing of the catheters in lab environment which, to the best of our knowledge, has not been performed before in literature. Although sensitivity analysis by adding random noises are also carried out in this study, the algorithms need to be extensively evaluated for medical application with clinical data which will be part of the future work.

The main contribution of this paper is to extend the 3D reconstruction approach of quadratic curves in closed form without the requirement of point-to-point correspondence for practical real-time shape sensing of catheters. In addition, this paper explores implementation issues for real-time execution and experimentally evaluates its accuracy, speed, and performance. The proposed algorithms are defined in general form that are potentially applicable to generic imaging modalities, including optical and x-ray cameras at arbitrary locations and to surgical applications like electrophysiology and interventional cardiology with round cross section cardiac catheters. In the following section, the proposed 3D reconstruction method is described. Section 3 provides details about image processing algorithms, experimental setup, procedure and results, followed by discussion and conclusion remarks sections.

2. Methods

2.1. Reconstruction algorithm

The 3D reconstruction algorithm proposed in this research is based on the reconstruction of a quadratic curve representing the 3D shape of the catheter centerline from two arbitrary perspective projections (Safaee-Rad *et al* 1992, Xie and Thonnat 1992, Kanatani and Liu 1993, Xie 1994, Kahl and Heyden 1998, Balasubramanian *et al* 2002). The schematic description of the proposed shape reconstruction algorithm is illustrated in figure 1. The proposed method consists of four main steps (figure 1). The first step is pre-processing of the two images acquired from the cameras. The second step is to extract the centerline points of the catheter (which is a round shape tube) from the two images using image processing techniques. The third step is to (1) find the actual positions of the centerline points on the image planes of the two cameras with respect to their coordinate frames; (2) determine the parameters of the 3D

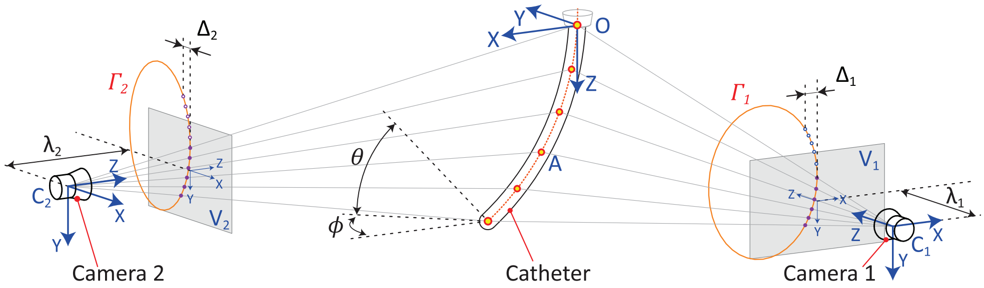

Figure 1. Schematic description of the proposed 3D reconstruction algorithm.

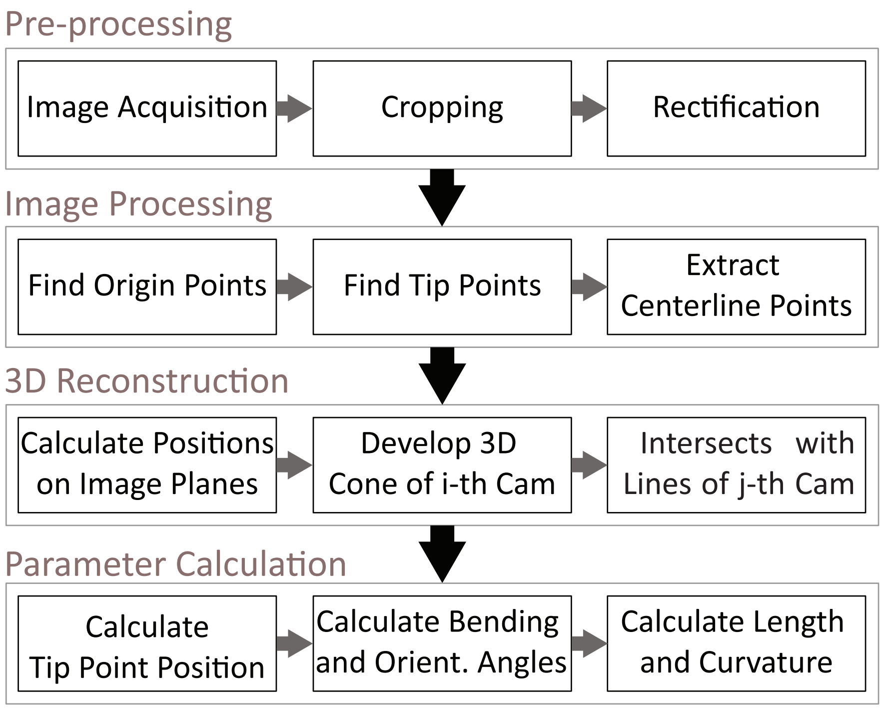

Figure 2. Block diagram of the proposed high speed vision-based algorithm for catheter 3D reconstruction.

cone whose vertex is at the focal point of one of the cameras and passes through the points on the image plane of this camera; and (3) obtain the analytical solutions for the intersection points of this cone with the ray lines of the other camera.

This combination of ray lines and cone avoids the need for accurate point correspondence between the two images. Techniques are developed here to choose the more appropriate camera for developing the 3D cone and also to choose the right intersection point that belongs to the centerline of the catheter. The fourth step is to, based on the obtained centerline points of the catheter, reproduce the 3D shape of the catheter and extract its parameters including curvature, length, bending and orientation angles, and tip position.

The schematic description of a general stereo imaging system is illustrated in figure 2. Reference frame $Oxyz$ is located at point O which is the fixed point of the catheter centerline. C_{ixyz} $(i = 1, 2)$ is the rectangular cartesian coordinate of the ith camera with its origin at the focal point of the camera (points C_i). Plane V_i is the virtual image plane of the ith camera. To simplify the projection problem and produce unrotated images, the virtual image planes are located in front of cameras. These planes are positioned at the distance λ_i from the center of projection of the ith camera. It should be noted that λ_i is also the homogeneous scaling factor of the ith camera. Pose of the cameras are assumed to be known with respect to each other using well-known stereo calibration methods (Bouguet 2015). Point A ($[X\ Y\ Z]^T$) is an arbitrary point in R^3 from the centerline of the catheter that is in the field of view of both cameras. Point A projected on the virtual image plane of the ith camera is denoted by A_{v_i} with pixel position $[X_{I_i}\ Y_{I_i}]^T$.

Using the perspective projection model of a pin-hole camera (Zhang 1999), the position coordinates of the point A_{v_i} in R^3 with respect to C_{ixyz} are

$$\begin{cases} X_{v_i} = \left((X_{I_i} - c_{x_i}) - (Y_{I_i} - c_{y_i})\dfrac{\tau_i}{f_{y_i}}\right)\dfrac{Z_{v_i}}{f_{x_i}} \\ Y_{v_i} = (Y_{I_i} - c_{y_i})\dfrac{Z_{v_i}}{f_{y_i}} \\ Z_{v_i} = \lambda_i \end{cases} \quad i = 1, 2. \tag{1}$$

where f_{x_i} and f_{y_i} are the focal lengths for x and y dimensions expressed in pixel, $[c_{x_i}\ c_{y_i}]^T$ is the principal point, and τ_i is the skew coefficient defining the angle between the x and y pixel axes.

We made the assumption that the catheter shape can be well-approximated as a 3D quadratic curve, which has been validated in previous studies for polymer catheters actuated by pull wires (Camarillo *et al* 2008a, Jung *et al* 2014). In the Discussion section we consider relaxing this assumption. The perspective projection of the catheter centerline (Γ) is presented by quadratic curve Γ_i on the image plane of the ith camera (figure 2). The problem here is how to reconstruct the 3D quadratic curve Γ from the pair of its perspective projections Γ_i from the two cameras in real-time.

The best-fit quadratic curve Γ_i to the n projected points $A_{v_{in}}$ on the virtual image plane of the ith camera ($i = 1$, 2 and $n = 1, ..., N$) found using image processing methods appropriate to the imaging modality is determined by applying a least square technique (Halir and Flusser 1998). Section 3.1 gives an implementation for the image processing methods. The fitted ellipse of the ith camera image is in general form (Halir and Flusser 1998)

$$\begin{aligned} &E_{i_1}X_{v_i}^2 + E_{i_2}X_{v_i}Y_{v_i} + E_{i_3}Y_{v_i}^2 \\ &\qquad + E_{i_4}X_{v_i} + E_{i_5}Y_{v_i} + E_{i_6} = 0 \quad i = 1, 2, \end{aligned} \tag{2}$$

where parameters E_{i_k} for ($k = 1, ..., 6$) are constant. The equation of the line C_{iA} in 3D space is

$$\frac{{}^{C_i}X}{X_{v_i}} = \frac{{}^{C_i}Y}{Y_{v_i}} = \frac{{}^{C_i}Z}{\lambda_i} = r_i \quad i = 1, 2 \tag{3}$$

where $[{}^{C_i}X\ {}^{C_i}Y\ {}^{C_i}Z]^T$ is the position of the point A with respect to the coordinate frame of the ith camera (${}^{C_i}A$). From calibration

$${}^{C_i}A = {}^{C_i}T_{C_j}\,{}^{C_j}A \quad i = 1, 2 \quad j = \begin{cases} 1 & \text{if } i = 2 \\ 2 & \text{if } i = 1 \end{cases} \tag{4}$$

where ${}^{C_i}T_{C_j}$ is the homogenous transformation matrix of the coordination frame of the jth camera to that of the ith camera. By finding ${}^{C_i}X$, ${}^{C_i}Y$, and ${}^{C_i}Z$ from equation (4) and substituting into equation (3), parameters X_{v_i} and Y_{v_i} are derived as functions of ${}^{C_j}X$, ${}^{C_j}Y$, and ${}^{C_j}Z$

$$\begin{cases} X_{v_i} = F_1({}^{C_j}X, {}^{C_j}Y, {}^{C_j}Z) \\ Y_{v_i} = F_2({}^{C_j}X, {}^{C_j}Y, {}^{C_j}Z) \end{cases}$$
$$i = 1, 2 \quad j = \begin{cases} 1 & \text{if } i = 2 \\ 2 & \text{if } i = 1. \end{cases} \tag{5}$$

Combining equations (2) and (5) yields the equation of the 3D elliptical cone Φ_i with respect to the coordinate frame of the jth camera. The vertex of this cone is the focal point of the ith camera and its intersection with the virtual plane V_i is the ellipse Γ_i. The equation of this conic is

$$\begin{aligned} \Phi_i = {} & K_{i_1}\, {}^{C_j}X^2 + K_{i_2}\, {}^{C_j}Y^2 + K_{i_3}\, {}^{C_j}Z^2 \\ & + K_{i_4}\, {}^{C_j}X\, {}^{C_j}Y + K_{i_5}\, {}^{C_j}X\, {}^{C_j}Z + K_{i_6}\, {}^{C_j}Y\, {}^{C_j}Z \\ & + K_{i_7}\, {}^{C_j}X + K_{i_8}\, {}^{C_j}Y + K_{i_9}\, {}^{C_j}Z + K_{i_{10}} = 0 \\ & i = 1, 2 \quad j = \begin{cases} 1 & \text{if } i = 2 \\ 2 & \text{if } i = 1. \end{cases} \end{aligned} \tag{6}$$

where parameters K_{i_l} for (l = 1, ..., 10) are constant. Substituting parameters ${}^{C_j}X$, ${}^{C_j}Y$, and ${}^{C_j}Z$ derived from equation (3) as

$$\begin{cases} {}^{C_j}X = r_j X_{v_j} \\ {}^{C_j}Y = r_j Y_{v_j} \\ {}^{C_j}Z = r_j \lambda_j \end{cases} \quad j = \begin{cases} 1 & \text{if } i = 2 \\ 2 & \text{if } i = 1. \end{cases} \tag{7}$$

into equation (6) will reduce it to

$$\sum_{t=1}^{s} L_{i_t} r_j^{s-t} = 0 \quad \begin{cases} i = 1, 2 \\ s = 3 \end{cases} \quad j = \begin{cases} 1 & \text{if } i = 2 \\ 2 & \text{if } i = 1. \end{cases} \tag{8}$$

where parameters L_{i_t} for (t = 1, 2, 3) are

$$\begin{aligned} L_{i_1} = {} & K_{i_1} X_{v_j}^2 + K_{i_2} Y_{v_j}^2 + K_{i_4} X_{v_j} Y_{v_j} \\ & + K_{i_5} X_{v_j} \lambda_j + K_{i_6} Y_{v_j} \lambda_j + K_{i_3} \lambda_j^2 \\ L_{i_2} = {} & K_{i_9} \lambda_j + K_{i_7} X_{v_j} + K_{i_8} Y_{v_j} \\ L_{i_3} = {} & K_{i_{10}} \end{aligned}$$

Parameters L_{i_t} are functions of E_{ik}, ${}^{C_i}T_{C_j}$, and λ_i. Solving equation (8) for parameters r_j and combining the solutions with equation (7) yields the z coordinate of the points of intersection of the line C_{iA} and the elliptical cone Φ_i in 3D space with respect to the coordinate frame of the $j-th$ camera as

$$\begin{aligned} & {}^{C_j}Z_u = -\frac{\lambda_i\left(L_{i2} + U\sqrt{L_{i2}{}^2 - 4L_{i1}L_{i3}}\right)}{2L_{i1}} \\ & \begin{cases} i = 1, 2 \\ u = 1, 2 \end{cases} \quad j = \begin{cases} 1 & \text{if } i = 2 \\ 2 & \text{if } i = 1 \end{cases} \\ & U = \begin{cases} -1 & \text{if } u = 1 \\ 1 & \text{if } u = 2. \end{cases} \end{aligned} \tag{9}$$

It is clear in equation (9) that two intersection points exist. From figure 2, the closer point to the reference frame origin (point O) along the z axis of the jth camera coordinate is the right solution. Therefore, the z coordinate of the intersection point belonging to the centerline of the catheter is

$$ {}^{C_j}Z = \underset{\{{}^{C_j}Z_u : u=1,2\}}{\arg\min} \left| {}^{C_j}Z_u - {}^{C_i}Z_O \right| \tag{10} $$

where ${}^{C_j}\mathrm{O} = [{}^{C_j}X_O \; {}^{C_j}Y_O \; {}^{C_j}Z_O]^T$ is the coordinate of the reference frame origin with respect to the coordinate frame of the jth camera. Using equations (9) and (10), the x and y coordinates of the selected intersection point are

$$ \begin{cases} {}^{C_j}X = \dfrac{{}^{C_j}Z}{\lambda_i} X_{v_j} \\ {}^{C_j}Y = \dfrac{{}^{C_j}Z}{\lambda_i} Y_{v_j} \end{cases} i = 1, 2 \quad j = \begin{cases} 1 & \text{if } i = 2 \\ 2 & \text{if } i = 1. \end{cases} \tag{11} $$

Coordinates of the intersection point with respect to the reference frame at point O is then determined by applying the transformation matrix of the coordinate systems of the jth camera to the reference frame. At least four points are required to establish the mapping between the coordinate frames of the cameras with respect to the reference frame. Additional points can help reduce the effects of noise. Using same algorithm, other points of the ellipse of jth image can be used to obtain other points on the centerline and the best-fit curve representing the curvature of the catheter in 3D space. This curve will then be used to determine features of the catheter including length.

Either image of the cameras can be used to generate the cone, but selecting the quadratic segment with higher curvature reduces the effects of noise in the fitting process. A special case, of course, is when the catheter is in the form of a 3D straight line making the curvature identical to zero. The algorithm copes with this singular case by triangulating origin and tip points of the catheter and using them to find the length of the catheter along the straight line from the origin to the tip. In this case, the bending and orientation angles are both zero.

3. Experiments

In order to evaluate the accuracy and performance of the proposed algorithm, experiments were conducted using the experimental setup shown in figure 3(a). The stereo vision system consists of two webcams (Logitech Webcam C930e) capable of capturing 24 bit color images at the resolution of 1920×1080 pixels at 30 fps. An example of the raw images captured by the cameras are presented in figure 3. The image backgrounds are covered by blue felt to simplify image preprocessing for experimental validation. The cameras were calibrated and the intrinsic parameters (focal length, principle point, and lens distortion coefficients) as well as the extrinsic parameters (rotation and translation of each camera relative to each other and also to the reference frame) were determined (Bouguet 2015). The transformation matrix from the camera to the reference coordination frames were determined by using a least-square technique and triangulating multiple known locations in R^3 with respect to the reference coordination frame.

Mock-ups of catheter-shape tubes with known geometry were tested and the results were compared against the known curvature and geometry. The mock-ups were rapid-prototyped with lengths of 160 mm and circular cross sections with outer diameters of 12 mm (figure 3(d)). They were fabricated using a Connex500 3D printer (Stratasys) from VeroWhite (RGD835),

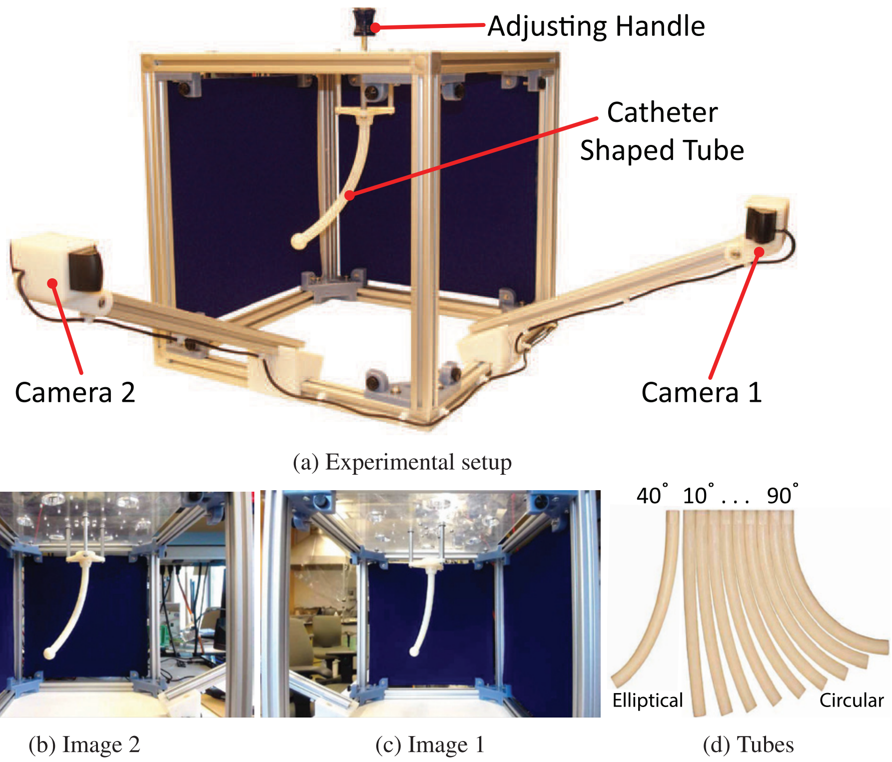

Figure 3. Developed system for evaluation of the proposed 3D reconstruction algorithm, examples of the images from both cameras and 3D printed circular and elliptical catheter shaped tubes with known shape. (a) Experimental setup. (b) Image sample from camera 2. (c) Image sample from camera 1. (d) Tubes.

a UV-cross-linkable acrylic polymer which is a high modulus ($\sim$1 GPa) plastic. The 3D printing accuracy specification is 20–85 μm for features below 50 mm and less than 200 μm for full model size. The backbone bending angles θ (figure 2) are from 10 to 90 deg for the circular-shape tubes and is 40 deg for elliptical-shape tube.

3.1. Centerline point extraction

As it is described in figure 1, the centerline points of the catheter in the two images serve as input for the 3D reconstruction step. Specifics will depend on modality (optical, x-ray, etc) and image characteristics. Several techniques to reproduce the centerline of the catheter-shape objects have been proposed in literature including SOM, detecting ridges using distance transform, calculating the Voronoi diagram and thinning using layer by layer erosion (Kumar *et al* 2004, Camarillo *et al* 2008b, Croom *et al* 2010). All of these techniques work well in practice. However, to lower the execution time of the image processing steps and allow continuous execution of reconstruction algorithms for evaluation purposes, customized algorithms were developed. The OpenCV library was employed to acquire images and perform image processing algorithms.

The image pre-processing procedure comprises of removing lens distortions from the images, cropping (figure 4(a)), thresholding and removing the blue backgrounds (figure 4(b)),

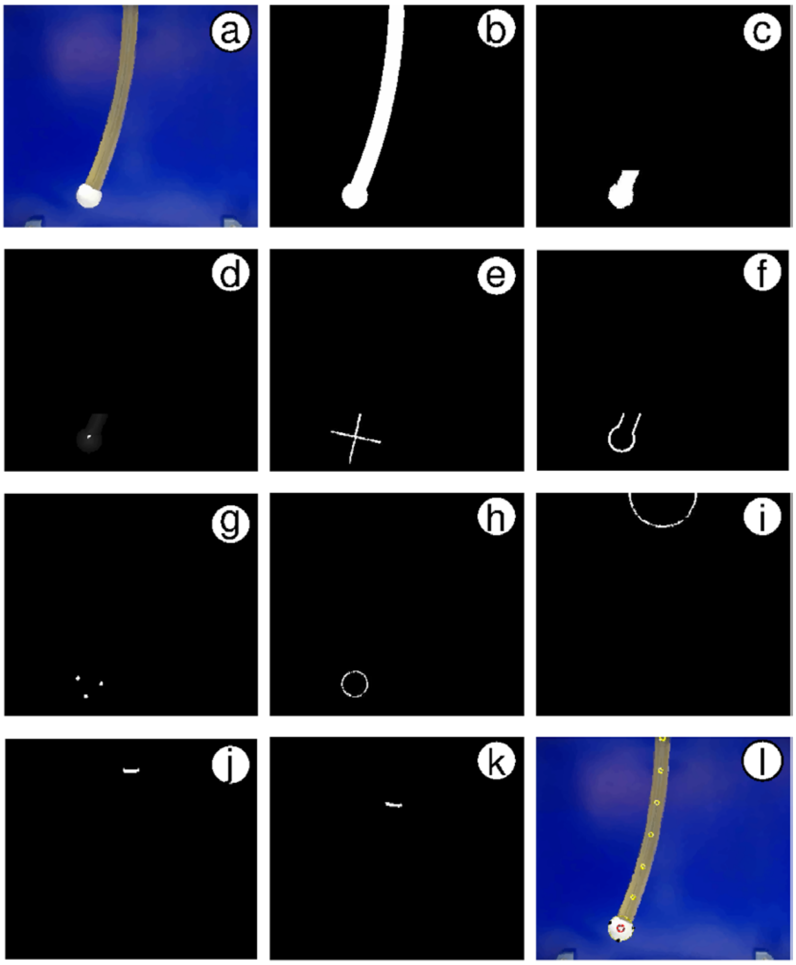

Figure 4. The snapshots of the image processing scene at different stages of the algorithm.

removing noise, and finding the position of the origin points by finding the location of the middle point of the the most top-right and most top-left white points in the images.

To find the tip point, the region of interest (ROI) of the tip (figure 4(c)) is found by detecting the most bottom white point in the binary image of the isolated catheter. The rough estimate of the tip point is then determined by applying distance transform to the ROI (figure 4(d)). A mask image containing the line joining the origin point to the estimated tip point and its perpendicular line at the tip point is then produced (figure 4(e)). By applying a bitwise AND operation of the Canny edge of the ROI (figure 4(f)) and the mask image, three points on the edge of the tip circle are obtained (figure 4(g)). These three points are then used to find the best-fit circle (figure 4(h)) which is located at the accurate position of the tip point. Once the tip point is detected, the tip circle is removed from the image in order to further isolate the catheter for the center line detection algorithm.

The centerline point extraction algorithm begins with applying a mask containing a circular arc centered at the origin point (figure 4(i)) to the binary images of the isolated catheter. This operation produces an image containing a small contour of the catheter in the form of

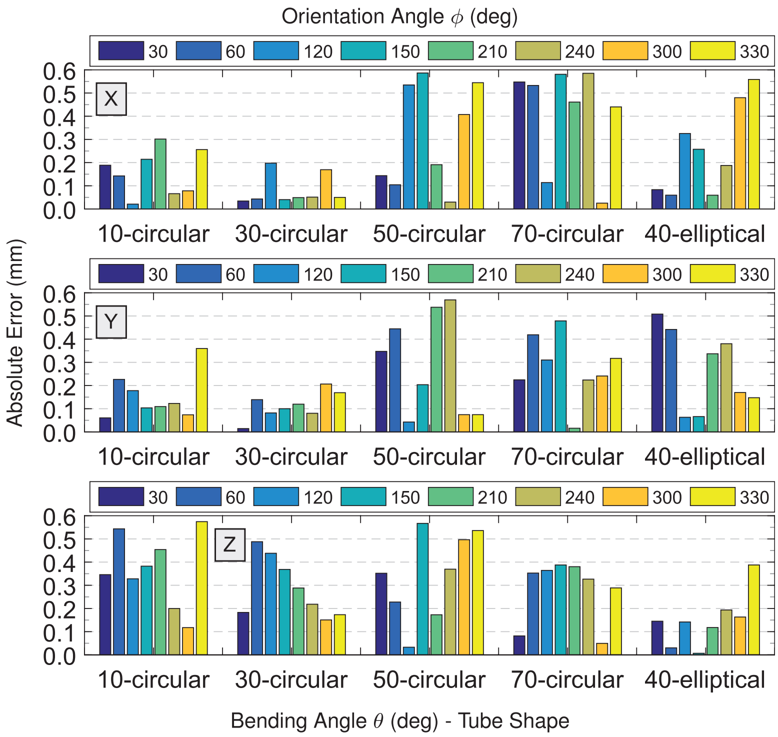

Figure 5. Absolute errors of x, y, and z coordinates of tip.

a circular arc (figure 4(j)). The center of mass of this contour belongs to the centerline of the catheter. This procedure continues by applying the same mask at the detected centerline point and finding the second circular arc (figure 4(k)) and centerline point. These operations are repeated until the area of the contour is zero. The number of the detected points can be adjusted by changing the radius of the circular arc used as the mask. The detected origin, tip, and centerline points (figure 4(l)) are then fitted to a quadratic curve, equation (2), using least square technique.

3.2. Experiment procedures

Two experiments were designed to validate the accuracy, precision and performance of the algorithms. In the first experiment, 3D printed circular catheter shaped tubes with the bending angles of 10, 30, 50, and 70 deg and an elliptical tube with the bending angle of 40 deg were tested. These mock-ups were manually positioned in the orientation angles ϕ (figure 2) of 30, 60, 120, 150, 210, 240, 300, and 330 deg and the image processing and reconstruction algorithms were performed. In the second experiment, the tubes with the bending angles of 10, 20, 30, 40, 50, 60, and 70 deg and the elliptical catheter-shape tube were tested by manually rotating them in front of the cameras while the proposed shape sensing algorithms was determining curvature and geometry of the tubes in real-time.

In the foregoing, clean images with sharp background were used to develop and evaluate the algorithm. However, in the clinical setting images are noisy. In order to evaluate the robustness of the proposed algorithm, sensitivity analysis was also carried out by determining the significance of the errors in catheter parameters caused by the inaccuracy in finding the

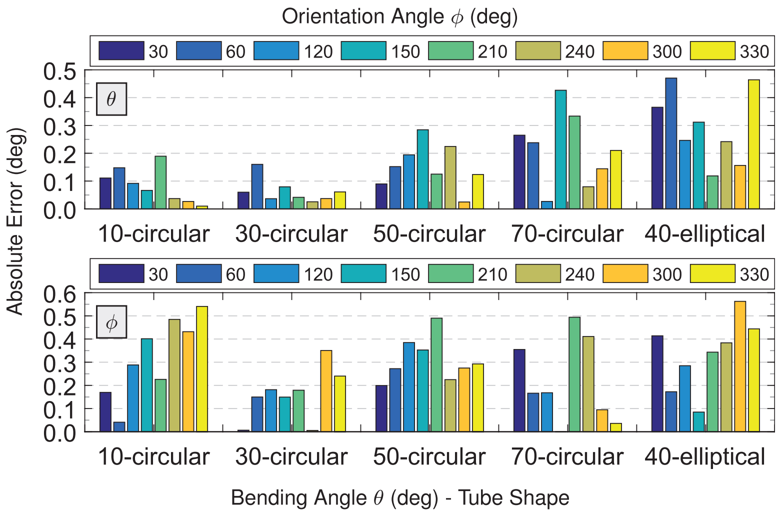

Figure 6. Absolute errors of bending and orientation angles.

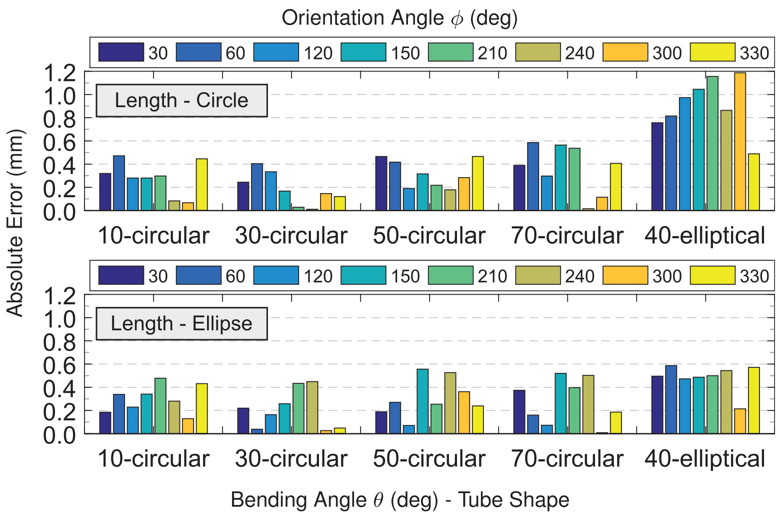

Figure 7. Absolute errors of catheter length.

catheter centerline points from the correspondence images. Random errors with the standard deviation (STD) of 1–6 mm (6 mm = catheter radius) were applied to the centerline points in both images, and the catheter parameters were obtained using the proposed reconstruction process. For each STD of the error, this procedure was repeated 1000 times for different set of randomly-generated errors. Bending angles of 10, 30, 50 and 70 were included in this analysis.

4. Results

Figures 5 and 6 present the absolute errors of the measured x, y, and z coordinates of the tip point and bending and orientation angles of the circular tubes for different bending and orientation angles in the first experiment, respectively from top to bottom. Absolute measurement

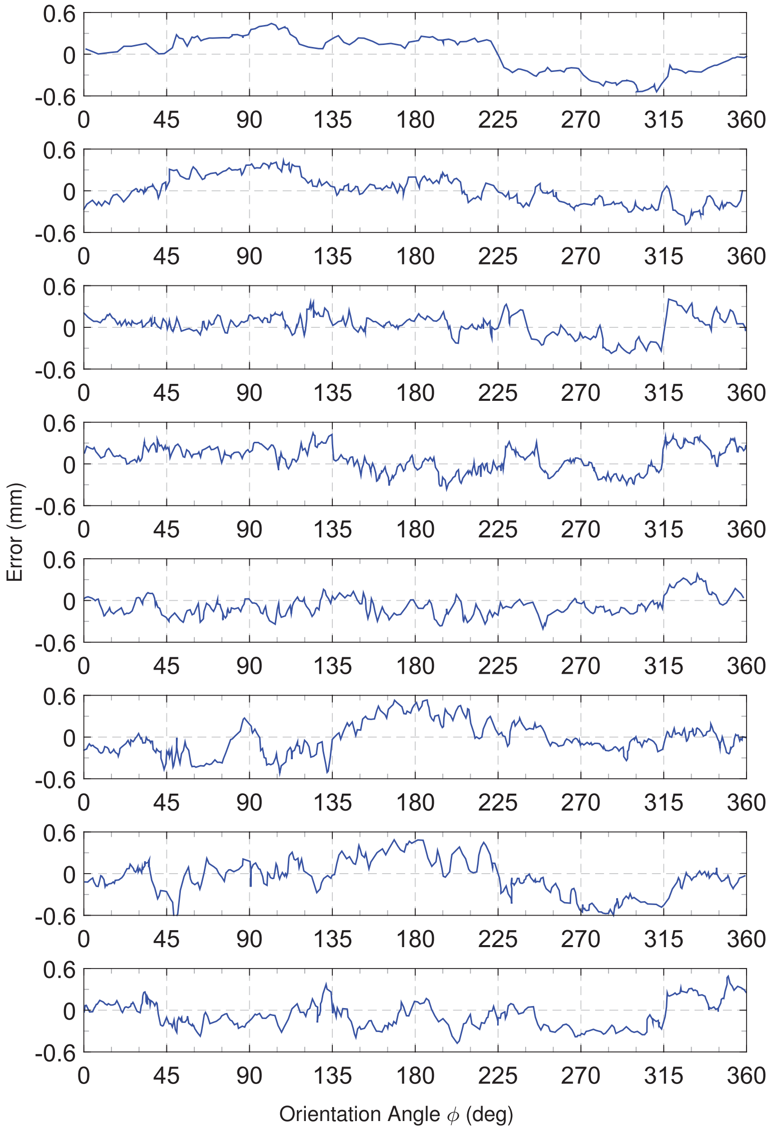

Figure 8. Measurement errors of z coordinate of the tip point in the second experiment for the circular tubes with the bending angles of 10–70 deg and the elliptical tube respectively from top to bottom.

errors of the length of the circular and elliptical tubes based on the fitted circles and ellipses are demonstrated in figure 7, respectively from top to bottom. From these figures, the measurement errors in all cases are very low. Errors in the x, y, and z coordinates of the tip (figure 5) are less than 0.6 mm and the measurement errors for the bending and orientation angles are less than 0.5 deg (figure 6). As presented in figure 7, the lengths of the circular catheter shaped tubes are similar for both fitted circles and ellipses with the maximum error of around 0.6 mm. However, in case of the elliptical shaped tube, the fitted ellipse demonstrates better accuracy compared to the fitted circle to the catheter centerline.

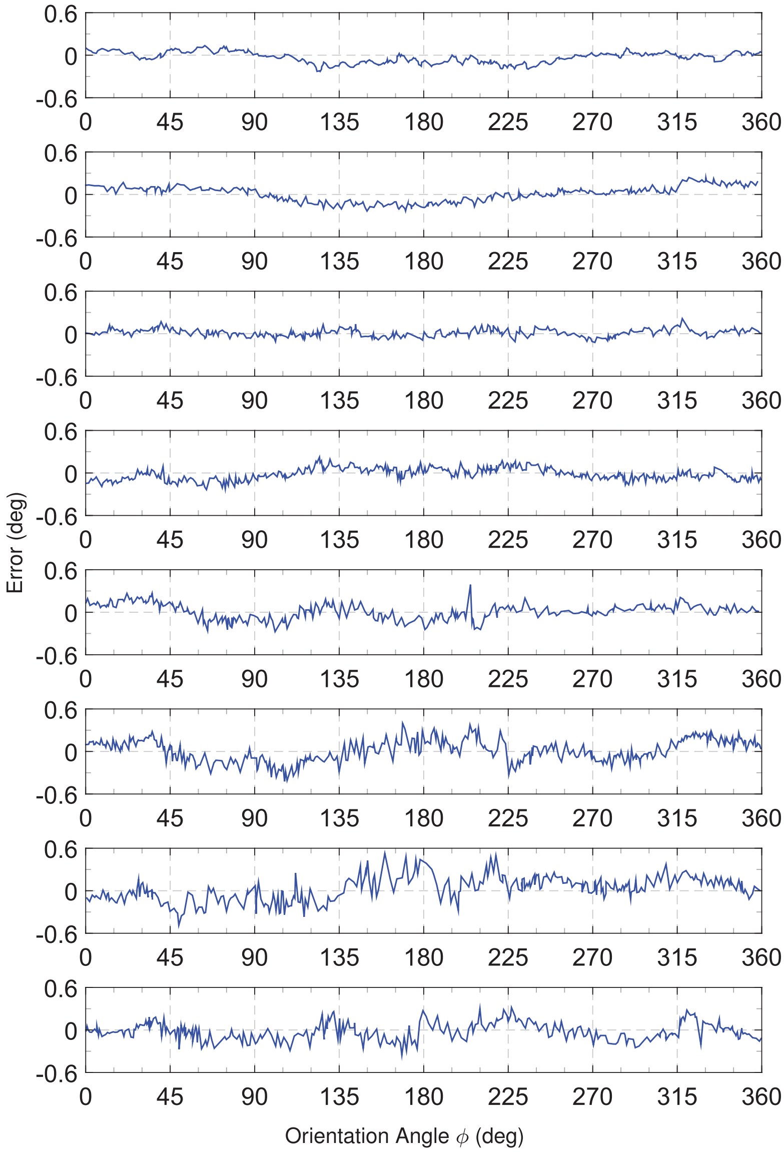

Figure 9. Measurement errors of the bending angles in the second experiment for the circular tubes with the bending angles of 10–70 deg and the elliptical tube respectively from top to bottom.

Figures 8–10 present the measurement errors in height of the tip point, bending angles, and length of the tubes based on the fitted circles and ellipses for the circular tubes with 10–70 deg bending angles and also for the elliptical tube for 0–360 deg orientation angles, respectively from top to bottom. A 3D plot of the tip points trajectories of the circular catheter shaped tubes with 10–70 deg bending angles obtained in the the second experiment is presented in figure 11.

In figures 5–10, the noise in the plots increases as the bending angle increases. This may be due to the radial distortion of the webcams which is greater in the areas far from the center

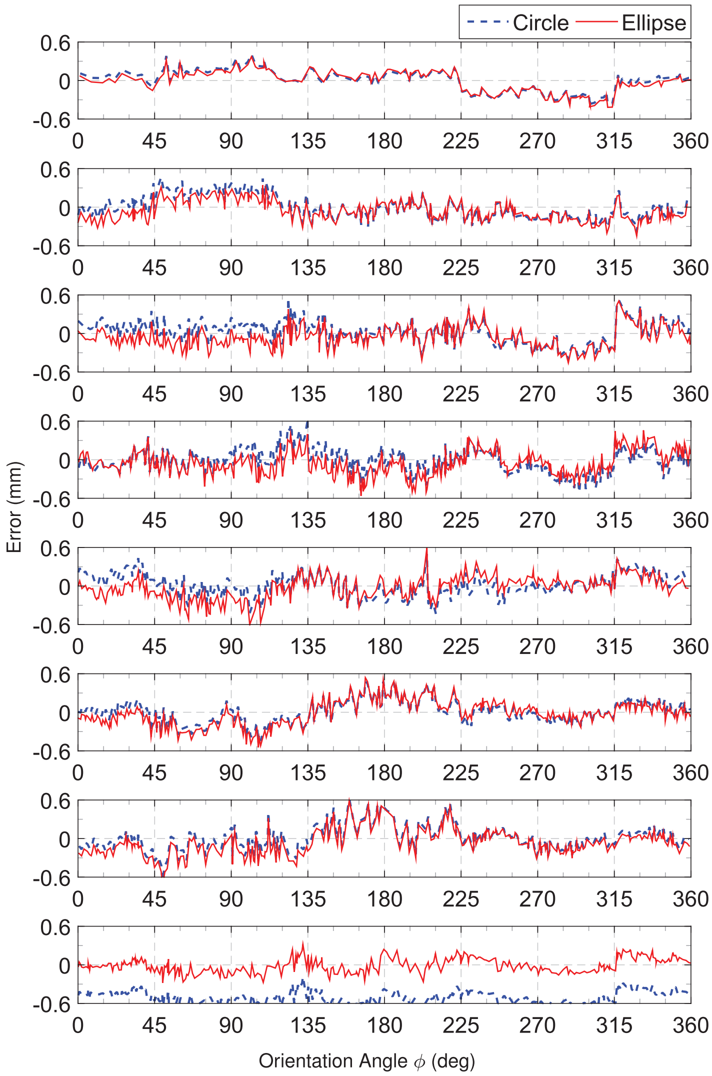

Figure 10. Errors of the tube lengths calculated in the second experiment based on the circles and ellipses fitted to the centerline points for the circular tubes with the bending angles of 10–70 deg and the elliptical tube respectively from top to bottom.

of the image plane. When the bending angle increases, the distance of the tip point from the center point also increases. Further calibration might reduce this error, however the error magnitudes are sufficiently small that this is likely unimportant for most applications.

Similar to the first experiment, the maximum errors of the measurement for the z coordinate of the tip point and for the bending angle are ± 0.6 mm and ± 0.5 deg, respectively. As seen in figure 10, the results calculated based on the fitted circles and ellipses are close for the circular-shape tubes. However, there are significant differences between the results for the elliptical shaped tube and the results based on the fitted ellipse has higher accuracy compared to those from the circle fitted to the centerline points of the tube. The mean absolute errors (MAE) across all conditions for both experiments are 0.24 mm for position and 0.21 deg for angular parameters.

Table 1. Mean and maximum absolute errors of the catheter parameters due to the added noise to the centerline points from the correspondence images.

Error type \ parameters	X (mm)	Y (mm)	Z (mm)	θ (deg)	ϕ (deg)	L (mm)
Mean absolute	0.3677	0.4093	0.3534	0.6793	0.9599	1.0840
Maximum	1.6865	1.7402	1.5871	2.6280	3.6486	2.4224

The execution time required for the entire image processing algorithms proposed here is measured to be 2.75 ms for two images with resolution of 1920×1080 pixels, and for the 3D reconstruction algorithm is measured to be 2.25 ms, implemented on a PC with Intel Core i7 processors running at 3.00 GHz with 16 Gb of memory. This allows a processing rate of around 200 fps, although, the web cameras used here are limited to 30 fps.

The results of the noise tests are presented in table 1. The mean and maximum absolute errors of the X, Y, Z coordinates of the catheter tip point as well as bending angle, bending plane angle and length of the catheter observed from 1000 trials for each STD error across all range of the STD errors and all bending angles are listed in this table. The mean absolute errors for tip position coordinates, angular parameters, and length of the catheter are less than 0.41 mm, 0.96 deg, and 1.1 mm, and the maximum absolute errors are 1.74 mm, 3.64 deg, and 2.42 mm, respectively. The results of this analysis suggests that the algorithm is reasonably robust to noise in the imaging and image processing process that determine the catheter centerline. This is because the 3D reconstruction algorithm uses information from the entire catheter length in finding the catheter's spatial shape. Errors that produce systematic errors over an extended segment of the catheter's length could results in significant additional error; this must be taken into account by ensuring that the image acquisition and image preprocessing steps are immune to this type of error.

5. Discussion

This study aimed to develop a method for using two images (typically optical or x-ray) to determine the shape of the bending section of an active catheter. Primary concerns were fast execution and good accuracy. The use of efficient image processing operations and analytical representations of the 3D reconstruction geometry enabled execution within 5 ms at 1920×1080 resolution, which is more than adequate for envisioned clinical applications (Camarillo *et al* 2008a, Kesner and Howe 2011). Simulations with added sensing error suggest that the proposed method is robust to moderately high noise levels, because the 3D reconstruction algorithm incorporates global information from throughout the catheter length. Although the algorithms are defined in general form, theoretically applicable to generic imaging modalities including optical and x-ray cameras at arbitrary locations, they need to be extensively evaluated for medical application with clinical data which will be part of future work. There are some potential anticipated limitations of the proposed system. One limitation is when the catheter is almost pointing toward one of the cameras which decreases the resolution as the catheters shaft approaches the camera. Repositioning the imaging system may be a solution for these cases. Image quality in older lower-resolution x-ray imaging systems may also be a limitation.

In clinical applications, operator input or cardiac and respiratory movements generate motion and deformation in the catheters. However, at an instant of time when the images are taken, they are effectively static images. Therefore, it is not needed to account for time. In order to get trajectories across time, this procedure is repeated. Since the proposed reconstruction

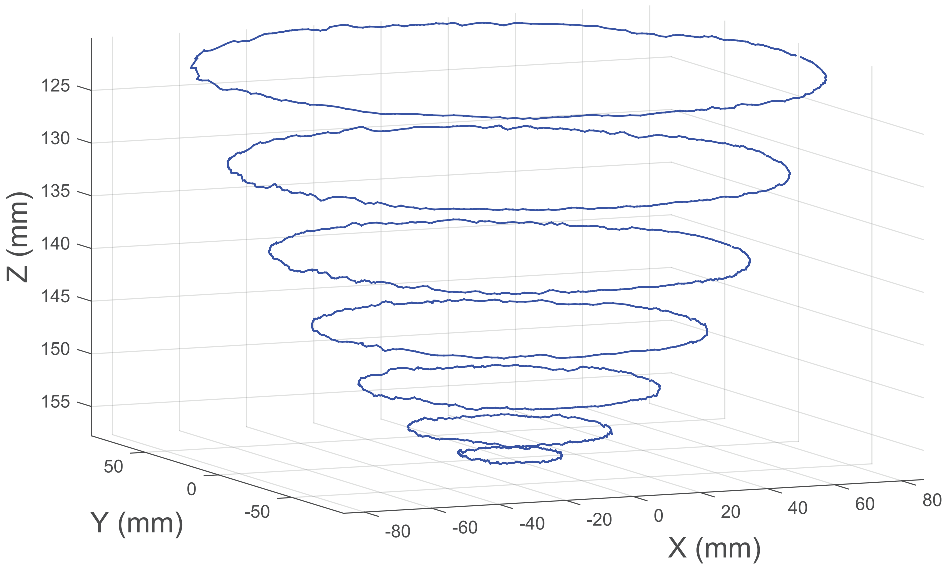

Figure 11. Tip point trajectories measured in the second experiment for the 10–70 deg circular tubes.

method can run at 200 Hz, we can reconstruct very fast movements by simply combining the images from the two views. So, no matter if the movements are due to the control system or due to cardiac and respiratory movements, the proposed algorithm is capable of reconstructing the shape of the catheter in real-time.

In surgical operations, there may be partial or sever overlaps on the catheter by other intracoronary devices or catheter shaped deformation due to the perspective projection in the acquired angiographic views (i.e. foreshortening effect). A solution to this problem, which is mainly an image processing challenge and is not the main focus of this work, may be to develop a system where initial manual designation of the catheter segment will allow the algorithm to keep track of the movements of the catheter. Although having more catheters and devices in the scene will increase the execution time of the process due to the multiple reconstruction process, the proposed reconstruction algorithm is not limited to one catheter as long as the centrelines of the catheters can be extracted from the images.

It is useful to compare the results from this study with alternate approaches in the literature, but this is in general challenging due to the large number of factors determining performance. These include software environment, processor speed, image modality and resolution, and constraints such as the use of fiducial markers. Here we provide a basic comparison with the performance of the most closely related vision-based algorithms for 2D/3D reconstruction of catheters/continuum robots/flexible manipulators. The reconstruction techniques presented in literature mainly were developed based on affine shape (iterative reconstruction) (Berthilsson and Astrom 1997), SOM (3D point cloud) (Croom *et al* 2010), voxel-carving algorithm (shape-from-silhouette) (Camarillo *et al* 2008b), epipolar correspondence points (brute force search) (Lee and Poston1997), or detection of the tip- or body-mounted fiducial markers (Chen *et al* 2003, Hannan and Walker 2003, 2005, Chitrakaran *et al* 2004, Webster *et al* 2009, Rucker 2011). Some of the reported accuracy-related results of these approaches (from 0.24 to 3.14 mm) are promising, however low speed (1.36–15 fps), dependency on

Table 2. Criteria for real-time vision-based shape sensing of catheter systems.

Design criteria \ author(s)	Rucker (2011)	Lee and Poston(1997)	Hannan and Walker (2005)	Camarillo *et al* (2008b), (2009)	Berthilsson and Astrom (1997), Berthilsson *et al* (1997)	Webster *et al* (2009)	Martinsson *et al* (2007)	Hong *et al* (2004)	Croom *et al* (2010)	This study
1. Computationally fast (>30 fps)	○	✗	✓	✗	○	✗	○	✗	✗	✓
2. Reasonably accurate (± 1 mm)	✗	○	○	✓	○	○	✓	○	✗	✓
3. No dependency to >2 cameras	✓	✓	✓	✗	✗	✓	✗	✓	✓	✓
4. No dependency to fiducial markers	✗	✓	✗	✓	✓	✗	✓	✓	✓	✓
5. No dependency to physical grid	✓	✓	✓	✓	✓	✗	✓	✓	✓	✓
6. No dependency to initial guess	✓	✓	✓	✓	✓	✓	✓	✓	✗	✓
7. No approximation by circular arcs	○	○	✗	✓	○	✗	○	○	✓	✓
8. Ability to find tip position	✓	○	✓	✓	○	✓	○	○	✗	✓
9. 3D Reconstruction capability	✓	✓	✗	✓	✓	✓	✓	✓	✓	✓

✓ = Meets criteria ✗ = Does not meet criteria ○ = Unknown or not applicable tip- or body-mounted fiducial markers, physical grids, or high number of required cameras/images (2 to 20) restrict their capabilities for high speed applications like motion compensation cardiac catheters. In terms of the accuracy and speed, the main factors that are limiting the reconstruction process in these approaches are high number of images necessary for the reconstruction process (Berthilsson and Astrom 1997, Berthilsson *et al* 1997, Martinsson *et al* 2007) or the reconstruction technique itself that can be inheritably time-consuming and computationally expensive. Higher spatial resolution or frame rate do not have positive impacts on these approaches and, in fact, they may further slow down the process. In terms of practical usage, besides the challenges in the central point extraction of the marker bands using image processing techniques, complex and difficult fabrication processes of the fiducial markers that meet size, shape and visibility constraints may be required. Overall, the results presented in this paper represent better overall performance than the published performance of alternative approaches. Furthermore, an informal analysis suggests that these approaches are unlikely to provide significantly better performance under similar conditions. Definitive comparison, however, would require implementation of the competing approaches and testing on identical image inputs, but this is beyond the scope of this study.

A list of important criteria for real-time tracking systems are defined in table 2. Our main goal in this research is the development and evaluation of a vision-based system that fulfills all or most of these design criteria. Amongst these criteria, the first two, namely speed and accuracy, are the most important. As presented in table 2, previous studies were largely unable to fulfil these requirements together.

In the developed experimental setup, the two cameras were mounted almost perpendicularly to each other. However, the proposed algorithm has no dependency on orthogonality and, in fact, they may be installed at any angle possible in a stereo vision system. Sensitivity to camera relative orientation can be determined through analysis of equations (10) and (11). Further studies are required to quantitatively analyse the effects of the viewing angle of the cameras on the accuracy of the proposed 3D reconstruction algorithm.

This study used specialized image processing algorithms, which must be adapted for surgical applications. Likewise, the 'catheter' in the validation experiments were oversized and used a ball tip. These implementation allowed the experiments to focus on the 3D shape estimation performance. The results demonstrated that the 3D algorithm itself was successful, with small error magnitudes in position, angle, and length. To evaluate the effectiveness and accuracy of the proposed algorithm, single segment catheter shaped tubes were tested. However, the proposed algorithm can be extended for the shape sensing of continuum robots with multiple segments and non-quadratic shapes using high order polynomial curves or by combining multiple quadratic curves.

6. Conclusion

In this paper, a vision-based shape sensing algorithm for real-time 3D reconstruction of catheters using two arbitrary perspective views based on the closed-form analytical solution for the reconstruction of quadratic curves in 3D space was presented. Using the closed-form analytical formation led to a high speed 3D reconstruction algorithm with no iteration involved that decreased the execution time to 2.25 ms. This allows the high process rate around 200 Hz that includes the processing time for the image processing algorithms as well. The experimental results demonstrated the maximum absolute measurement errors of 0.6 mm for the tip position and 0.5 deg for the angular parameters including bending and orientation of the catheter shaped rapid-prototyped circular and elliptical tubes with known geometry and curvature.

The MAE across all conditions were measured 0.24 mm for position and 0.21 deg for angular parameters. The results of sensitivity analysis demonstrated reasonable robustness of the algorithm to the added noise in the images. The speed, accuracy, and lack of dependency on body-mounted fiducial markers makes it a potential solution for a variety of medical imaging sources including biplane fluoroscopy and stereo endoscopy. In future, the proposed reconstruction algorithm will be further evaluated with clinical data and will also be used in an automated catheter system for position control and measurement of the catheters.

References

Alterovitz R, Branicky M and Goldberg K 2008 Motion planning under uncertainty for image-guided medical needle steering *Int. J. Robot. Res.* **27** 1361–74

Andruska A M and Peterson K S 2008 Control of a snake-like robot in an elastically deformable channel *IEEE/ASME Trans. Mechatronics* **13** 219–27

Balasubramanian R, Das S and Swaminathan K 2002 Reconstruction of quadratic curves in 3-D from two or more perspective views *Math. Probl. Eng.* **8** 207–19

Bender H-J, Männer R, Poliwoda C, Roth S and Walz M 1999 Reconstruction of 3D catheter paths from 2D x-ray projections *Medical Image Computing and Computer-Assisted Intervention* (New York: Springer) pp 981–9

Berthilsson R and Astrom K 1997 Reconstruction of 3d-curves from 2d-images using affine shape methods for curves *Proc. IEEE Computer Society Conf. on Computer Vision and Pattern Recognition* pp 476–81

Berthilsson R, Åström K and Heyden A 1997 Projective reconstruction of 3d-curves from its 2d-images using error models and bundle adjustments *Proc. of the Scandinavian Conf. on Image Analysis* vol 2 pp 581–8 (Proceedings Published By Various Publishers)

Bouguet J-Y 2015 Camera calibration toolbox for matlab (online) available: www.vision.caltech.edu/bouguetj/calib_doc/index.html

Burgner J, Rucker D C, Gilbert H B, Swaney P J, Russell P T, Weaver K D and Webster R J 2014 A telerobotic system for transnasal surgery *IEEE/ASME Trans. Mechatronics* **19** 996–1006

Camarillo D B, Milne C F, Carlson C R, Zinn M R and Salisbury J K 2008a Mechanics modeling of tendon-driven continuum manipulators *IEEE Trans. Robot.* **24** 1262–73

Camarillo D B, Loewke K E, Carlson C R and Salisbury J K 2008b Vision based 3D shape sensing of flexible manipulators *IEEE Int. Conf. on Robotics and Automation* pp 2940–7

Camarillo D B, Carlson C R and Salisbury J K 2009 Configuration tracking for continuum manipulators with coupled tendon drive *IEEE Trans. Robot.* **25** 798–808

Chen J, Behal A, Dawson D and Fang Y 2003 2.5D visual servoing with a fixed camera *Proc. of the American Control Conf.* vol 2 pp 3442–7

Chitrakaran V K, Behal A, Dawson D M and Walker I D 2004 Setpoint regulation of continuum robots using a fixed camera *IEEE Proc. of the in American Control Conf.* vol 2 pp 1504–9

Croom J M, Rucker D C, Romano J M and Webster R J 2010 Visual sensing of continuum robot shape using self-organizing maps *IEEE Int. Conf. on Robotics and Automation* pp 4591–6

Cusano A, Breglio G, Giordano M, Nicolais L and Cutolo A 2004 Multifunction fiber optic sensing system for smart applications *IEEE/ASME Trans. Mechatronics* **9** 40–9

Ding J, Goldman R E, Xu K, Allen P K, Fowler D L and Simaan N 2013 Design and coordination kinematics of an insertable robotic effectors platform for single-port access surgery *IEEE/ASME Trans. Mechatronics* **18** 1612–24

Fritzke B 1996 Unsupervised ontogenetic networks *Handbook of Neural Computation* (Bristol: IOP)

Glozman D and Shoham M 2007 Image-guided robotic flexible needle steering *IEEE Trans. Robot.* **23** 459–67

Grattan K T V and Sun T 2000 Fiber optic sensor technology: an overview *Sensors Actuators* A **82** 40–61

Gravagne I A, Rahn C D and Walker I D 2003 Large deflection dynamics and control for planar continuum robots *IEEE/ASME Trans. Mechatronics* **8** 299–307

Haase C, Schäfer D, Dössel O and Grass M 2014 3D ablation catheter localisation using individual C-arm x-ray projections *Phys. Med. Biol.* **59** 6959

Halir R and Flusser J 1998 Numerically stable direct least squares fitting of ellipses *Proc. 6th Int. Conf. in Central Europe on Computer Graphics and Visualization* vol 98 pp 125–32

Hannan M and Walker I 2003 Vision based shape estimation for continuum robots *Proc. IEEE Int. Conf. on Robotics and Automation* vol 3 pp 3449–54

Hannan M W and Walker I D 2005 Real-time shape estimation for continuum robots using vision *Robotica* **23** 645–51

Hannan M W and Walker I D 2001 Analysis and experiments with an elephant's trunk robot *Adv. Robot.* **15** 847–58

Hong W, Ma Y and Yu Y 2004 Reconstruction of 3D symmetric curves from perspective images without discrete features *Computer Vision-ECCV 2004* (New York: Springer) pp 533–45

Jones B A and Walker I D 2006 Kinematics for multisection continuum robots *IEEE Trans. Robot.* **22** 43–55

Jung J, Penning R S and Zinn M R 2014 A modeling approach for robotic catheters: effects of nonlinear internal device friction *Adv. Robot.* **28** 557–72

Kahl F and Heyden A 1998 Using conic correspondences in two images to estimate the epipolar geometry *6th Int. Conf. on Computer Vision* pp 761–6

Kallem V and Cowan N J 2007 Image-guided control of flexible bevel-tip needles *IEEE Int. Conf. on Robotics and Automation* pp 3015–20

Kallem V and Cowan N J 2009 Image guidance of flexible tip-steerable needles *IEEE Trans. Robot.* **25** 191–6

Kanatani K and Liu W 1993 3D interpretation of conics and orthogonality *CVGIP: Image Understand.* **58** 286–301

Kesner S B and Howe R D 2011 Position control of motion compensation cardiac catheters *IEEE Trans. Robot.* **27** 1045–55

Kohonen T 1990 The self-organizing map *Proc. IEEE* **78** 1464–80

Kumar G S, Kalra P K and Dhande S G 2004 Curve and surface reconstruction from points: an approach based on self-organizing maps *Appl. Soft Comput.* **5** 55–66

Lee W-S and Poston T 1997 Rapid 3D tube reconstruction from nearby views *5th Int. Conf. in Central Europe in Computer Graphics and Visualization* pp 262–71

Lee J, Sponberg S N, Loh O Y, Lamperski A G, Full R J and Cowan N J 2008 Templates and anchors for antenna-based wall following in cockroaches and robots *IEEE Trans. Robot.* **24** 130–43

Leleu S, Abou-Kandil H and Bonnassieux Y 2001 Piezoelectric actuators and sensors location for active control of flexible structures *IEEE Trans. Instrum. Meas.* **50** 1577–82

Ma Y L, Shetty A K, Duckett S, Etyngier P, Gijsbers G, Bullens R, Schaeffter T, Razavi R, Rinaldi C A and Rhode K S 2012 An integrated platform for image-guided cardiac resynchronization therapy *Phys. Med. Biol.* **57** 2953

Martinsson H, Gaspard F, Bartoli A and Lavest J-M 2007 Reconstruction of 3d curves for quality control *Image Analysis: 15th Scandinavian Conf., SCIA 2007 (Aalborg, Denmark, 10–14 June 2007)* (Berlin: Springer) pp 760–9

Ning K and Worgotter F 2012 Control system development for a novel wire-driven hyper-redundant chain robot, 3D-trunk *IEEE/ASME Trans. Mechatronics* **17** 949–59

Park Y-L, Elayaperumal S, Daniel B, Ryu S C, Shin M, Savall J, Black R J, Moslehi B and Cutkosky M R 2010 Real-time estimation of 3D needle shape and deflection for MRI-guided interventions *IEEE/ASME Trans. Mechatronics* **15** 906–15

Panayiotou M, King A P, Ma Y, Housden R J, Rinaldi C A, Gill J, Cooklin M, O'Neill M and Rhode K S 2013 A statistical model of catheter motion from interventional x-ray images: application to image-based gating *Phys. Med. Biol.* **58** 7543

Panayiotou M, Rhode K S, King A P, Ma Y, Cooklin M, O'Neill M, Gill J, Rinaldi C A and Housden R J 2015 Image-based view-angle independent cardiorespiratory motion gating and coronary sinus catheter tracking for x-ray-guided cardiac electrophysiology procedures *Phys. Med. Biol.* **60** 8087

Polygerinos P, Seneviratne L D, Razavi R, Schaeffter T and Althoefer K 2013 Triaxial catheter-tip force sensor for MRI-guided cardiac procedures *IEEE/ASME Trans. Mechatronics* **18** 386–96

Roesthuis R J, Kemp M, van den Dobbelsteen J J and Misra S 2014 Three-dimensional needle shape reconstruction using an array of fiber bragg grating sensors *IEEE/ASME Trans. Mechatronics* **19** 1115–26

Rucker D C 2011 The mechanics of continuum robots: model—based sensing and control *PhD Dissertation* Vanderbilt University

Safaee-Rad R, Tchoukanov I, Benhabib B and Smith K C 1992 3D-pose estimation from a quadratic-curved feature in two perspective views *Proc. 11th IAPR Int. Conf. on Pattern Recognition. Vol 1. Conf. A: Computer Vision and Applications* pp 341–4
Trivedi D, Rahn C D, Kier W M and Walker I D 2008 Soft robotics: biological inspiration, state of the art, and future research *Appl. Bionics Biomech.* **5** 99–117
Webster R J, Memisevic J and Okamura A M 2005 Design considerations for robotic needle steering *Proc. of the IEEE Int. Conf. on Robotics and Automation* pp 3588–94
Webster R J, Kim J S, Cowan N J, Chirikjian G S and Okamura A M 2006 Nonholonomic modeling of needle steering *Int. J. Robot. Res.* **25** 509–25
Webster R J, Swensen J P, Romano J M and Cowan N J 2009 Closed-form differential kinematics for concentric-tube continuum robots with application to visual servoing *Experimental Robotics* (New York: Springer) pp 485–94
Xie M 1994 On 3D reconstruction strategy: a case of conics *Proc. of the 12th IAPR Int. Conf. on Pattern Recognition. Vol 1—Conf. A: Computer Vision & Image Processing* vol 1 pp 665–7
Xie M and Thonnat M 1992 A theory of 3D reconstruction of heterogeneous edge primitives from two perspective views *Computer Vision-ECCV'92* (New York: Springer) pp 715–9
Yang J, Cong W, Chen Y, Fan J, Liu Y and Wang Y 2014 External force back-projective composition and globally deformable optimization for 3D coronary artery reconstruction *Phys. Med. Biol.* **59** 975
Zhang Z 1999 Flexible camera calibration by viewing a plane from unknown orientations *The Proc. of the 7th IEEE Int. Conf. on Computer Vision* vol 1 pp 666–73